

Cite this: DOI: 10.1039/c1sm06219k

www.rsc.org/softmatter

COMMUNICATION

Three dimensional aspects of droplet coalescence during dropwise condensation on superhydrophobic surfaces†

Konrad Rykaczewski,^{*a} John Henry J. Scott,^a Sukumar Rajauria,^{bc} Jeff Chinn,^d Amy M. Chinn^d and Wanda Jones^d

Received 29th June 2011, Accepted 5th August 2011

DOI: 10.1039/c1sm06219k

We report formation of nano-to-microscale satellite droplets in the geometrical shadow of high contact angle primary drops during dropwise water condensation on a nanostructured superhydrophobic surface (SHS). The primary drops contribute to the heat transfer process by sweeping up satellite droplets without covering their nucleation site and thus allow for rapid condensation of multiple droplets from the same site.

Understanding of the dynamics of self propelled dropwise condensation occurring on natural^{1–3} and artificial^{4–9} superhydrophobic surfaces (SHS) is fundamentally important for improving the heat transfer efficiency in applications such as energy generation, micro-electronic thermal management,¹⁰ and fog harvesting.¹¹ On these surfaces, individual droplets emerge out of a $\approx 2 \mu\text{m}$ to $\approx 4 \mu\text{m}$ wetted area between the nanostructures. The droplets initially grow mainly by increasing their contact angle until reaching a nearly spherical shape with a diameter between $\approx 4 \mu\text{m}$ and $\approx 6 \mu\text{m}$.^{12,13} Next, the droplets grow in a near constant contact angle mode^{12,13} while remaining in an immobile Wenzel state.¹⁴ Drops with diameters larger than $25 \mu\text{m}$ ^{9,15} can depart the surface without application of an external force^{3,16,17} by coalescing with another large drop^{4,5,9,15} and forming a new drop in the mobile Cassie-Baxter state.¹⁸ In this work, we utilize *in situ* Environmental Scanning Electron Microscopy (ESEMTM)† to show that high contact angle primary drops can project over growing nano-to-microscale satellite droplets. Furthermore, the primary drops sweep up the satellite droplets without covering their nucleation site, allowing for rapid condensation of multiple satellite droplets from the same nucleation site. We discuss the impact of this coalescence mechanism on the drop size distribution and heat transfer during the condensation process.

^aMaterial Measurement Laboratory, National Institute of Standards and Technology, Gaithersburg, MD, 20899-8320, USA. E-mail: konrad.rykaczewski@nist.gov

^bCenter for Nanoscale Science and Technology, National Institute of Standards and Technology, Gaithersburg, MD, 20899-8320, USA

^cMaryland Nanocenter, University of Maryland, College Park, MD, 20740, USA

^dIntegrated Surface Technologies, Inc., 1455 Adams Dr., Ste 1125, Menlo Park, CA, 94025, USA

† Electronic Supplementary Information (ESI) available: Movies corresponding to condensation processes. See DOI: 10.1039/c1sm06219k/

We study water condensation occurring on a microscopically flat, nanostructured SHS. The surface comprises Al_2O_3 nanoparticles¹⁹ formed by the oxidation reaction of $2\text{Al}(\text{CH}_3)_3 + 3 \text{H}_2\text{O} \rightarrow \text{Al}_2\text{O}_3 + 6\text{CH}_4$ deposited onto a silicon wafer. To form a durable SHS, alkyl bridge silanes were used to create silsesquioxane structures which encapsulated the nano-particles into a glass like matrix. The nano-composite was then surface-modified with a perfluorinated silane coating²⁰ (see Fig. 1a). The entire SHS film was created at room temperature. The droplet condensation is achieved in the ESEMTM by decreasing the sample temperature below the saturation temperature (0°C to 7°C) corresponding to the chamber vapour pressure of 700 Pa to 900 Pa (5 Torr to 7 Torr). To avoid any electron beam heating effects,¹² the drops are imaged with a low electron beam energy of 10 keV and current of 0.16 nA. The process is imaged with a 512 pixel by 471 pixel resolution and a frame time of 250 ms and corresponding images are captured with a 5 Hz frequency. Images captured with 20° and 90° sample tilt (Fig. 1b and c) show that water condensation on the nanostructured SHS results in formation of nearly spherical drops with diameters ranging from $\approx 5 \mu\text{m}$ to

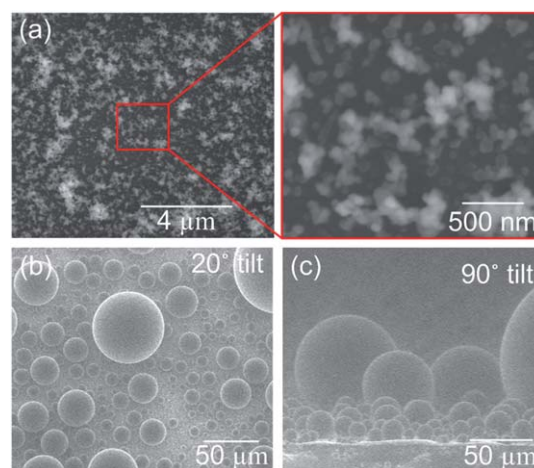


Fig. 1 (a) ESEMTM images of the SHS consisting of Al_2O_3 nanoparticles encapsulated in a glass-like matrix deposited onto a silicon wafer and modified with a perfluorinated silane coating. To prevent charging, samples were imaged in Low Pressure mode with water vapour of 67 Pa, electron beam energy of 10 keV and spot size 4; (b) 20° and (c) 90° sample tilt ESEMTM images of dropwise condensation on the SHS.

$\approx 300 \mu\text{m}$. We observe continual shedding of the larger drops from the surface under both orientations, which is in agreement with previous reports.^{4,7,9} Importantly, we do not observe degradation of the superhydrophobic characteristics of the surface during sustained dropwise condensation over multiple ESEMTM sessions lasting several hours each.

A close examination of top down images of the condensation process reveals growth of small satellite droplets partially in the geometrical shadow of large primary drops. Fig. 2a shows a top down example of a primary drop with $\approx 30 \mu\text{m}$ diameter (d_p) projecting over multiple satellite droplets with diameters (d_s) between $\approx 4 \mu\text{m}$ to $\approx 7 \mu\text{m}$. The side view in Fig. 2b clearly reveals the three dimensional nature of this coalescence mechanism. The satellite droplet emerges out of a wetted area between the nanostructures that is $\approx 4 \mu\text{m}$ across and mainly grows by increasing its contact angle

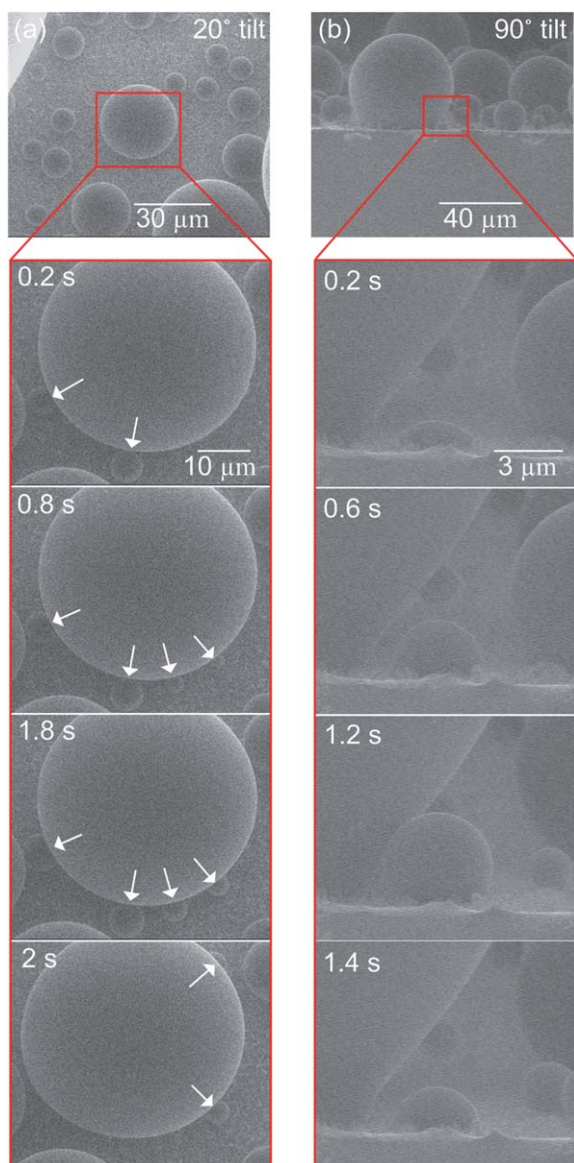


Fig. 2 Time sequence of (a) 20° and (b) 90° tilt ESEMTM images of dropwise condensation on the nanostructured superhydrophobic surface highlighting the growth of nano-to-microscale satellite drops (location indicated by white arrows) in the shadow of the primary drops.

until reaching a height of $\approx 5 \mu\text{m}$. Because the nucleation site is below the liquid-air interface of the primary drop, the satellite droplet has a constrained growth cavity and cannot grow any further without contacting and coalescing with the primary drop. Because the coalescence event adds an almost negligible volume to the primary drop (0.5% for coalescence of secondary and primary drops with $d_s = 5 \mu\text{m}$ and $d_p = 30 \mu\text{m}$), the liquid to solid contact line does not appreciably move. As a result, the satellite droplet nucleation site located $\approx 5 \mu\text{m}$ from the liquid to solid contact line is not covered by the primary drop and can facilitate nucleation of additional satellite droplets. The time required for coalescence depends on the location and size of the nucleation site with respect to the primary drop liquid to solid contact line and is on the order of a few seconds.

To quantify the described coalescence mechanism we measured the heights (h_s) and the diameters of a sequence of satellite droplets growing and coalescing out the nucleation site shown in Fig. 2 (see schematic in Fig. 3a for definition of h_s and d_s).[§] As shown in Fig. 3a, the satellite droplet grows with a significant increase in h_s and a moderate increase in d_s prior to coalescing. To capture the increase of both of these variables in one parameter, we report the calculated volume as a function of time (shown in the lower right hand side inset in Fig. 3a). The graph in Fig. 3b shows that eleven satellite droplets formed and coalesced with the primary drop within eleven seconds. The ESEMTM image in Fig. 3b shows that this rapid droplet growth and coalescence process ends when the primary drop covers the preferred nucleation site. In general, we observe that 5 to 15 satellite droplets can grow from the same nucleation site before it is covered by the primary drop (see Fig. 3d). The reason for repeated sequential satellite droplet growth out of the same nucleation site is not clear and depends on whether immediately after the coalescence event the area previously occupied by the satellite drop is dry or partially wetted. Because water drop coalescence occurs extremely fast,²¹ we cannot capture such details of the dynamics of the coalescence event with the ESEMTM. If the nucleation site surface is left dry, the preferential water condensation implies that the surface is locally more hydrophilic.²² In contrast, if the nucleation site surface is left partially wetted, vapour can directly condense onto the surface of the liquid water. Thus the satellite droplet growth can proceed without first wetting the area between the nanostructures^{12,13} and can occur faster. The microscale size of the droplets could give rise to effects such as negative Laplace pressure in the capillary bridge^{23,24} forming between the drops and makes a more concrete theoretical explanation of the dynamics of the coalescence and satellite droplet dewetting challenging.

The data in Fig. 3c indicate that the satellite droplet needs to have a diameter three to four times smaller than that of the primary drop (the slope of the linear fit to the outlying points in Fig. 3c is 0.287 ± 0.053)[§] for the rapid coalescence mechanism to be active. For example, multiple droplets with d_s of $\approx 2 \mu\text{m}$ and $\approx 5 \mu\text{m}$ can grow and coalesce with drops with d_p of $\approx 9 \mu\text{m}$ and $\approx 20 \mu\text{m}$, respectively. However, coalescence of a $\approx 5 \mu\text{m}$ and a $\approx 10 \mu\text{m}$ diameter drops is likely to cover both of the nucleation sites. The relative drop diameter criterion for the rapid growth and coalescence mechanism can be easily explained by evaluating the increase in the diameter and the volume of drops before and after merging. By assuming fully spherical drops we can estimate that coalescence of a satellite droplet with $d_s = 1/3 d_p$ will enlarge the volume of the primary drop by 3.7%, allowing for multiple coalescence events to occur without significant expansion of the primary drop. At this relative ratio, 14 such

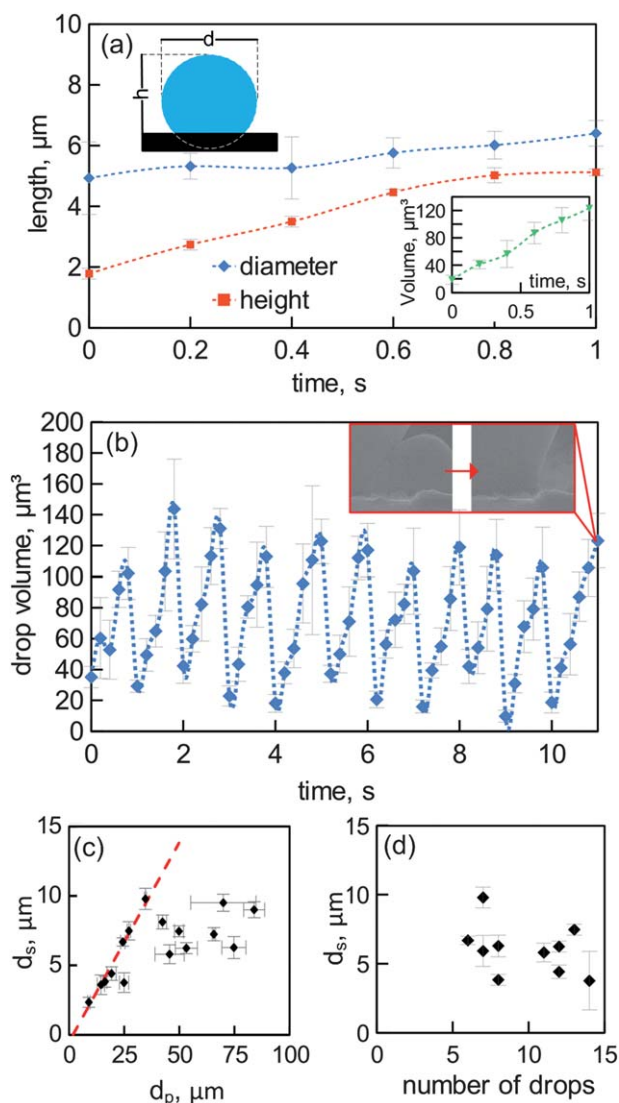


Fig. 3 (a) Example satellite droplet diameter and height as a function of time; the inset in the right lower corner shows the corresponding plot for computed drop volume as a function of time, (b) Drop volume as a function of time for multiple droplets growing from same nucleation site; the inset shows that eventually the primary drop covers the nucleation site, (c) Satellite droplet diameter (d_s) vs. primary drop diameter (d_p) for pairs of drops for which the rapid coalescence mechanism involving several drops was observed, and (d) Diameter of satellite droplets (d_s) vs. number of the satellite droplets growing from the same nucleation site before covering of the site by the primary drop.

coalescence events would be required to increase the primary drop size (50% volume and 15% d_p increase) so that it could cover the nucleation site (ex. $\approx 5 \mu\text{m}$ for d_p of $\approx 30 \mu\text{m}$). In contrast, coalescence of a satellite droplet $d_s = \frac{1}{2} d_p$ will enlarge d_p by 12.5%, thus resulting in about 50% volume and 15% d_p increase within only 4 coalescence events. We observe the mechanism occurring with d_p ranging from $\approx 10 \mu\text{m}$ to $\approx 85 \mu\text{m}$ (the mechanism is also likely to occur in the vicinity of primary drops with d_p up to the maximum $\approx 300 \mu\text{m}$ but is difficult to observe experimentally), but only with d_s smaller than about $10 \mu\text{m}$. For satellite droplets with d_s larger than $10 \mu\text{m}$ (for example a $20 \mu\text{m}$ diameter satellite growing near a $100 \mu\text{m}$ diameter primary drop) growth occurs slowly predominantly by

coalescence with other satellite droplets, making multiple growth and coalescence events from the same nucleation site unlikely.

To gain insight into how the droplet coalescence mechanism described in this work will influence the heat transfer during the process, we compare the characteristics of coalescence events occurring on a nanostructured SHS and a flat hydrophobic surface. In dropwise condensation most of heat transfer from the vapour to the substrate occurs by nucleation and growth of sub- $10 \mu\text{m}$ drops.^{25–28} As indicated schematically in Fig. 4, the large droplets do not significantly contribute to the heat transfer because of their large overall heat transfer resistance. As a result the portion of the substrate surface covered by the large drops is considered largely inactive.²⁹ For a coalescence event between a primary and a satellite droplet to occur during dropwise condensation on a flat hydrophobic surface the liquid to solid contact lines for the two drops must overlap.³⁰ Such coalescence event is likely to result in covering of the nucleation site by the primary drop and increasing the size of the inactive section of the substrate. In contrast, during dropwise condensation occurring on a nanostructured SHS the large primary drops can eliminate numerous micron scale droplets from the surface without covering the preferred nucleation site. As a result, the primary drops condensed on a nanostructured SHS, unlike primary drops with the same wetted base area condensed on a flat hydrophobic surface, actively contribute to the heat transfer process by sweeping up sub- $10 \mu\text{m}$ diameter droplets as they grow, thus enabling more condensation to occur. Consequently, over the same time period, significantly more sub- $10 \mu\text{m}$ diameter droplets will condense on the nanostructured SHS than on the hydrophobic surface. Experimental quantification of increase in the number of small drops is difficult

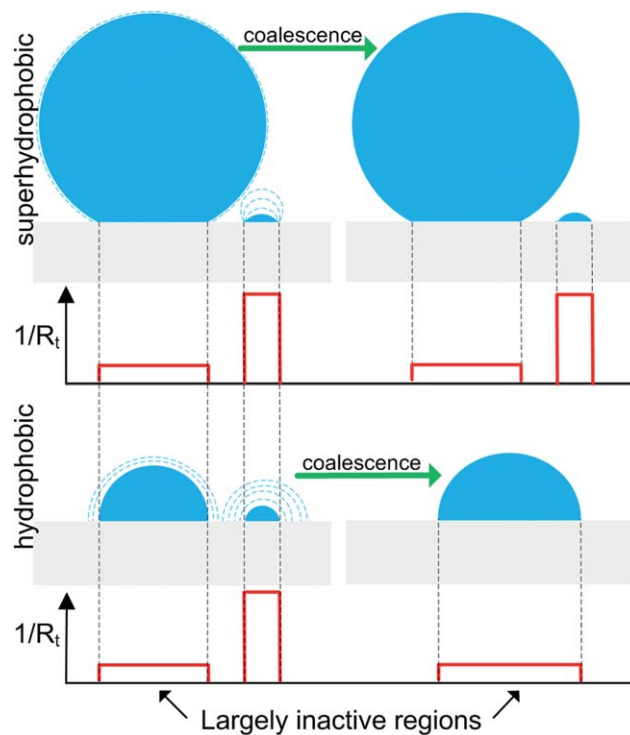


Fig. 4 Schematic contrasting droplet coalescence and local heat transfer resistances for dropwise condensation occurring on a nanostructured superhydrophobic and flat hydrophobic surfaces. R_t represents the local overall heat transfer resistance.

because the satellite droplets grow rapidly in the geometric shadow of the primary drops. However, based on our experimental results we expect this previously unaccounted shift in the drop size distribution towards smaller sizes to be significant enough to increase the heat transfer coefficient for this phase change process.

In summary, we describe a novel droplet coalescence mechanism during dropwise condensation on a superhydrophobic surface. Specifically, using *in situ* ESEMTM we reveal that as many as fifteen sub-10 μm satellite droplets can sequentially form from the same nucleation site and coalesce with a primary drop. The current mechanism is different from the drop formation below a large drop resting on top of hydrophobic micropillars^{31,32} and should occur on any surface (with and without microstructure) which retains superhydrophobic characteristics during condensation. This rapid coalescence mechanism occurs when the coalescing satellite droplet diameter is below $\approx 10 \mu\text{m}$ and is three to four times smaller than the primary droplet for primary drop diameters ranging from $\approx 10 \mu\text{m}$ to $\approx 85 \mu\text{m}$. The main impact of this coalescence mechanism has not been accounted for previously: an increase in the number of condensed sub-10 μm droplets. This work provides direct experimental evidence for the industrial benefits of SHS and should serve as a further motivation for development of economical ways to manufacture durable and robust coatings,^{33,34} which unlike most surfaces with water contact angles above 150° (as measured by the sessile drop technique) produced to date,^{31,32,35–45} retain their superhydrophobic characteristics during condensation and can be applied to promote continuous self propelled dropwise condensation on an industrial scale.

Acknowledgements

This research was performed while K. Rykaczewski held a National Research Council American Recovery and Reinvestment Act (NRCARRA) Research Associateship at the National Institute of Standards and Technology in Gaithersburg, MD. Support for this work by Integrated Surface Technologies was provided in part by the National Science Foundation under grant IIP-1026571.

Notes and references

‡ Certain commercial equipment, instruments, and materials are identified in this publication to adequately specify the experimental procedure. Such identification in no way implies approval, recommendation, or endorsement by NIST, nor does it imply that the equipment, instruments, or materials identified are necessarily the best available for the purpose.

§ The captured images are analyzed using the ImageJ analysis software package. All reported values of the diameter, d , and the height, h , are averages of six measurements with associated standard error (σ_d and σ_h corresponding to standard deviation d and h). The volume of the spherical cap, V , is calculated according to $V = 0.333\pi h^2(1.5d - h)$ with corresponding standard error, σ_V , calculated according to the formula $\sigma_V = (((\pi h d - \pi h^2)\sigma_h)^2 + (0.5\pi h^2\sigma_d)^2)^{0.5}$. All reported uncertainties are calculated with a coverage factor of 2. The linear fit in Fig. 3c was calculated using the R statistical data analysis package with a variance weighted least squares method.

- 1 B. Mockenhaupt, H.-J. Ensikat, M. Spaeth and W. Barthlott, *Langmuir*, 2008, **24**, 13591–13597.
- 2 Y. M. Zheng, D. Han, J. Zhai and L. Jiang, *Appl. Phys. Lett.*, 2008, **92**, 084106.
- 3 J. B. Boreyko and C. H. Chen, *Phys. Rev. Lett.*, 2009, **103**, 174502.
- 4 C. H. Chen, Q. J. Cai, C. L. Tsai, C. L. Chen, G. Y. Xiong, Y. Yu and Z. F. Ren, *Appl. Phys. Lett.*, 2007, **90**, 173108.
- 5 C. Dorrer and J. Ruhe, *Adv. Mater.*, 2008, **20**, 159–163.
- 6 K. K. S. Lau, J. Bico, K. B. K. Teo, M. Chhowalla, G. A. J. Amaratunga, W. I. Milne, G. H. McKinley and K. K. Gleason, *Nano Lett.*, 2003, **3**, 1701–1705.
- 7 C. Dietz, K. Rykaczewski, A. G. Fedorov and Y. Joshi, *Appl. Phys. Lett.*, 2010, **97**, 033104.
- 8 Q. Ke, S. Zhang, T. Tang, S. Wang and H. Jing, *Colloids Surf., A*, 2011, **377**, 110–114.
- 9 J. B. Boreyko and C. H. Chen, *Phys. Rev. Lett.*, 2009, **103**, 184501.
- 10 N. A. Patankar, *Soft Matter*, 2010, **6**, 1613–1620.
- 11 H. G. Andrews, E. A. Eccles, W. C. E. Schofield and J. P. S. Badyal, *Langmuir*, 2011, **27**, 3798–3802.
- 12 K. Rykaczewski, J. H. J. Scott and A. G. Fedorov, *Appl. Phys. Lett.*, 2011, **98**, 093106.
- 13 K. Rykaczewski and J. H. J. Scott, *ACS Nano*, 2011, **5**, 5926–5968.
- 14 R. N. Wenzel, *Ind. Eng. Chem.*, 1936, **28**, 988–994.
- 15 F.-C. Wang, F. Yang and Y.-P. Zhao, *Appl. Phys. Lett.*, 2011, **98**, 053112.
- 16 T. N. Krupenkin, J. A. Taylor, T. M. Schneider and S. Yang, *Langmuir*, 2004, **20**, 3824–3827.
- 17 G. Liu, L. Fu, A. V. Rode and V. S. J. Craig, *Langmuir*, 2011, **27**, 2595–2600.
- 18 A. B. D. Cassie and S. Baxter, *Trans. Faraday Soc.*, 1944, **40**, 546–551.
- 19 M. T. Swihart, *Curr. Opin. Colloid Interface Sci.*, 2003, **8**, 127–133.
- 20 J. Chinn, F. Helmrich, R. Guenther, M. Wiltse, K. Hurst and R. W. Ashurst, in *NSTI-Nanotech 2010*, 2010, vol. 1.
- 21 D. G. A. L. Aarts, H. N. W. Lekkerkerker, H. Guo, G. H. Wegdam and D. Bonn, *Phys. Rev. Lett.*, 2005, **95**, 164503.
- 22 K. K. Varanasi, M. Hsu, N. Bhate, W. Yang and T. Deng, *Appl. Phys. Lett.*, 2009, **95**, 094101.
- 23 S. H. Yang, M. Nosonovsky, H. Zhang and K.-H. Chung, *Chem. Phys. Lett.*, 2008, **451**, 88–92.
- 24 S. Yang, H. Zhang, M. Nosonovsky and K.-H. Chung, *Langmuir*, 2008, **24**, 743–748.
- 25 L. R. Glicksman and A. W. Hunt, *Int. J. Heat Mass Transfer*, 1972, **15**, 2251–2269.
- 26 C. Graham and P. Griffith, *Int. J. Heat Mass Transfer*, 1973, **16**, 337–346.
- 27 J. W. Rose, *Int. J. Heat Mass Transfer*, 1967, **10**, 755–765.
- 28 J. W. Rose, *Proc. Inst. Mech. Eng., Part A*, 2002, **216**, 115–128.
- 29 V. P. Carey, *Liquid-Vapor Phase-Change Phenomena*, 2nd edn, Taylor and Francis, New York, 2008.
- 30 S. Anand and S. Y. Son, *Langmuir*, 2010, **26**, 17100–17110.
- 31 R. D. Narhe and D. A. Beysens, *Langmuir*, 2007, **23**, 6486–6489.
- 32 C. Dorrer and J. Ruhe, *Langmuir*, 2007, **23**, 3820–3824.
- 33 Y. C. Jung and B. Bhushan, *ACS Nano*, 2009, **3**, 4155–4163.
- 34 T. Verho, C. Bower, P. Andrew, S. Franssila, O. Ikkala and R. H. A. Ras, *Adv. Mater.*, 2011, **23**, 673–678.
- 35 A. Lafuma and D. Quere, *Nat. Mater.*, 2003, **2**, 457–460.
- 36 C. Dorrer and J. Ruhe, *Langmuir*, 2007, **23**, 3179–3183.
- 37 K. A. Wier and T. J. McCarthy, *Langmuir*, 2006, **22**, 2433–2436.
- 38 R. D. Narhe and D. A. Beysens, *Europhys. Lett.*, 2006, **75**, 98–104.
- 39 R. D. Narhe, W. González-Viñas and D. A. Beysens, *Appl. Surf. Sci.*, 2010, **256**, 4930–4933.
- 40 R. D. Narhe and D. A. Beysens, *Phys. Rev. Lett.*, 2004, **93**, 076103.
- 41 Y.-T. Cheng and D. E. Rodak, *Appl. Phys. Lett.*, 2005, **86**, 144101.
- 42 Y. C. Jung and B. Bhushan, *J. Microsc.*, 2008, **229**, 127–140.
- 43 M. Nosonovsky and B. Bhushan, *Langmuir*, 2007, **24**, 1525–1533.
- 44 M. Nosonovsky and B. Bhushan, *Nano Lett.*, 2007, **7**, 2633–2637.
- 45 M. He, J. Wang, H. Li and Y. Song, *Soft Matter*, 2011, **7**, 3993–4000.